Timing and Frequency Synchronization for OFDM Downlink Transmissions Using Zadoff-Chu Sequences

Malik Muhammad Usman Gul, Xiaoli Ma, *Senior Member, IEEE*, and Sungeun Lee

***Abstract*—Orthogonal frequency division multiplexing (OFDM) technique has been widely adopted in wireless systems, but it is known for being sensitive to synchronization errors. In this paper, we present timing and frequency synchronization algorithms for OFDM downlink transmissions using Zadoff-Chu sequences. We show that the current timing synchronization method employing Zadoff-Chu sequences is sensitive to carrier frequency offsets. To reduce this sensitivity, we develop conditions for the selection of appropriate Zadoff-Chu sequences. We then design a training sequence and propose joint signal detection, timing, and carrier frequency offset estimation algorithms for OFDM downlink transmissions. We show that the proposed schemes simplify the overall synchronization architecture and improve the performance compared to the existing schemes in the literature.**

***Index Terms*—Orthogonal frequency division multiplexing (OFDM), synchronization, carrier frequency offset, timing offset, channel estimation, Zadoff-Chu sequence.**

I. Introduction

ORTHOGONAL frequency division multiplexing (OFDM) is a multi-carrier transmission technique with applications in numerous wireless communication systems such as IEEE 802.11n [1], IEEE 802.16m [2], long term evolution-advanced (LTE-A) [3], and digital video broadcasting [4]. The granularity in frequency (sub-carrier) and time (OFDM symbols) domains in OFDM enables efficient multi-user resource utilization while one-tap equalization reduces the complexity of broad-band transmissions. However, a major challenge in OFDM systems is to achieve reliable timing and frequency synchronization because improper synchronization can result in inter-symbol interference (ISI) and inter-carrier interference (ICI), which severely degrade system performance [5]. Timing synchronization deals with the estimation and the tracking of timing offsets (TO) caused by random propagation delays and/or a sampling frequency mismatch between the transmitter and the receiver. In addition, frequency synchronization deals with the estimation and the compensation of carrier frequency offset (CFO) between the transmitter and the receiver because of oscillator mismatch and/or the Doppler effect. To simplify timing synchronization and reduce ISI and ICI due to multipath channel, a cyclic prefix (CP) is appended at the beginning of each OFDM symbol. As CP is always longer than the maximum excess delay of the channel, some samples towards the end of CP are ISI-free. Hence, it is sufficient to estimate the start of the OFDM symbol within this ISI-free sample region [5].

Both timing and frequency synchronization are usually performed in two phases: coarse and fine [6]–[8]. Coarse timing synchronization generates an initial estimate of the starting index of the OFDM symbol within the CP while fine timing improves the estimate to a difference of few samples from the ideal starting point. Similarly, coarse frequency synchronization provides a rough CFO estimate while fine frequency synchronization estimates the residual CFO.

In cellular communications, synchronization begins on the downlink (DL) when a mobile-user (MU) synchronizes itself to a base-station (BS). As the MU has no prior synchronization information, CFO on the DL can be large. For example, in LTE DL transmissions with 2 GHz of carrier frequency and 15 kHz of sub-carrier spacing [3], a clock accuracy of ± 10 ppm (parts per million) can result in a maximum CFO of ± 20 kHz (1.33 sub-carrier spacings) at the MU. Therefore, fractional as well as integer CFOs can appear on the DL. As DL coarse timing synchronization usually precedes frequency synchronization, timing synchronization should be robust to integer CFOs. Once DL synchronization has been achieved, CFOs on the UL, caused only by residual synchronization errors and Doppler spread, are usually very small (fractional only) [9].

Various timing and frequency synchronization methods have been proposed in the literature that include both data-aided or training-assisted schemes [5]–[8], [10]–[20] and non-data-aided or blind schemes [21]–[28]. Non-data-aided methods use inherent structure of the OFDM symbol for synchronization. However, for satisfactory performance, these algorithms usually require a large number of OFDM symbols. In contrast, data-aided synchronization schemes employ either the auto-correlation of the received training symbol or its cross-correlation with the local copy at the receiver. Auto-correlation-based methods for timing synchronization [6], [11], [13], [15] use training symbols with repetitions that offer robustness to large CFO and multi-path channel. Therefore, these methods are suitable for coarse DL TO and CFO estimation. In the absence of CFO, cross-correlation-based methods [12], [17], [18] offer better timing synchronization performance and lower

Manuscript received October 23, 2013; revised April 8, 2014 and September 3, 2014; accepted November 2, 2014. Date of publication November 20, 2014; date of current version March 6, 2015. Part of this work was presented at the Conference on Information Sciences and Systems, Princeton, NJ, USA, March 2012. The associate editor coordinating the review of this paper and approving it for publication was A. Vosoughi.

The authors are with the School of Electrical and Computer Engineering, Georgia Institute of Technology, Atlanta, GA 30332 USA (e-mail: usman.gul@gatech.edu).

Color versions of one or more of the figures in this paper are available online at http://ieeexplore.ieee.org.

Digital Object Identifier 10.1109/TWC.2014.2372757

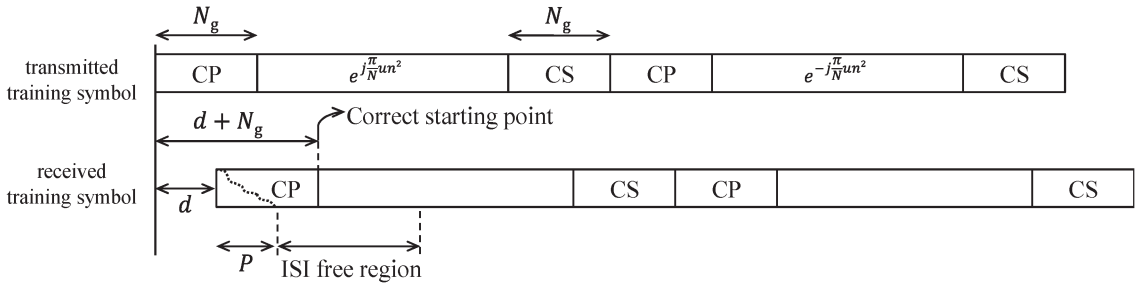

Fig. 1. Proposed training symbol and the corresponding ISI-free region for a timing offset of d samples.

probabilities of miss and false alarm. However, in the presence of integer CFOs, the performance of these methods degrades severely, which limits their use to fine timing estimation schemes [7], [8], [12], [17], which use auto-correlation-based algorithms for coarse timing and cross-correlation-based algorithms for fine timing estimation.

To facilitate synchronization and cell search procedures in LTE DL and UL, Zadoff-Chu (ZC) sequences [29] have been proposed as training symbols [3]. ZC sequences are part of the family of constant-amplitude zero auto-correlation (CAZAC) sequences in which circularly shifted copies of a sequence are uncorrelated [29]. Thus, ZC sequences are ideal candidates for UL timing synchronization because different users can transmit ZC sequences with different shifts, and TO estimation can be performed efficiently using cross-correlation with the primary ZC sequence. Recently, joint fine timing and channel estimation using ZC or general CAZAC sequences have been proposed for DL transmissions in [17], [18]. The algorithm uses a ZC sequence with a cyclic suffix (CS) in addition to the CP and shows that the cross-correlation with the received ZC sequence generates an estimate of the channel impulse response (CIR) that is further used to estimate fine timing of the OFDM symbol. However, the critical problems of CFO estimation and coarse timing synchronization in the presence of CFOs have not been addressed. Instead, the algorithm resorts to auto-correlation-based scheme [11] for coarse timing and CFO estimation that increases the complexity of the overall synchronization procedure.

In this paper, we propose novel cross-correlation-based joint timing and frequency synchronization schemes for DL transmissions that employ ZC sequences. We illustrate that non zero CFOs can affect the identifiability of TO estimation. Specifically, in the presence of integer CFOs, the cross-correlation peak shifts by an amount determined by the integer CFO and ZC sequence parameters. Exploring this relationship, we propose a training sequence containing two suitable ZC sequences, each with a CS in addition to the CP. We present the criterion for selection of appropriate ZC sequence parameters so that the cross-correlation peak lies within the ISI-free region for a certain maximum integer CFO, which allows coarse TO and CFO estimation. The CFO estimate is further used to improve the TO estimate. We also design a training signal detection test and calculate the threshold for training signal validation. Simulation results show that the proposed schemes offer robustness to large CFOs and better performance than the existing schemes in the literature. We also show that the ZC sequences used in LTE DL are not suitable for cross-correlation-based timing synchronization in the presence of large CFOs. With our proposed coarse synchronization schemes combined with [17], [18], a single cross-correlation-based hardware architecture can be used for signal detection and estimation of coarse and fine TO, integer CFO, and multi-path channel resulting in a significant reduction in hardware resource usage for practical implementations.

The rest of the paper is organized as follows. Section II presents the system model and the proposed training block. In Section III, we discuss the conventional cross-correlation-based timing synchronization employing ZC sequences and its sensitivity to CFOs. Section IV deals with the effect of integer CFOs and ZC sequence parameters on the cross-correlation. It also presents the criterion for the selection of appropriate ZC sequences for CFO robustness. Employing the appropriate ZC sequences, Section V presents the signal detection and coarse timing synchronization algorithms. After detection and TO estimation, Section VI presents the CFO estimation and TO refinement method. We present the simulation results in Section VII, and Section VIII contains the conclusions.

II. System Model

We consider a base-band equivalent system model of an OFDM DL transmission in which a transmitter (BS) transmits a training block to the receiver (MU). The training block contains two ZC sequences, each with a CP of N_{CP} samples and a CS of N_{CS} samples, as shown in Fig. 1. For simplicity, we take $N_{\mathrm{CP}} = N_{\mathrm{CS}} = N_{\mathrm{g}}$. The n^{th} sample of the training block is given as

$$x[n] = \begin{cases} e^{j\frac{\pi}{N}u(n-N_{\mathrm{g}})^2} & 0 \le n \le N_{\mathrm{t}} - 1, \\ e^{-j\frac{\pi}{N}u(n-N_{\mathrm{t}}-N_{\mathrm{g}})^2} & N_{\mathrm{t}} \le n \le 2N_{\mathrm{t}} - 1, \end{cases} \tag{1}$$

where N is the length of the ZC sequence, u is the root index relatively prime to N, and $N_{\mathrm{t}} = N + 2N_{\mathrm{g}}$. Note that the samples $x[n]$ for $0 \le n \le N_{\mathrm{g}} - 1$ and $N_{\mathrm{t}} \le n \le N_{\mathrm{t}} + N_{\mathrm{g}} - 1$ are the CP for the first and second ZC sequences, respectively. Similarly, $N + N_{\mathrm{g}} \le n \le N_{\mathrm{t}} - 1$ and $2N_{\mathrm{t}} - N_{\mathrm{g}} \le n \le 2N_{\mathrm{t}} - 1$ comprise the CS. We assume an even value of N here, but similar analysis can be carried out for odd N as well. Note that the second ZC sequence of the training block is the complex conjugate of the first sequence.

The received signal is sampled at a sampling frequency of $F_{\mathrm{s}} = N\Delta f$, where Δf is the sub-carrier spacing. The n^{th} sample of the received training block can be represented as

$$y[n] = e^{j\frac{2\pi}{N}fn} \sum_{p=0}^{P-1} h[p]x[n-d-p] + w[n], \tag{2}$$

where f is the CFO normalized by sub-carrier spacing, d is the TO in units of sample period ($\frac{1}{F_s}$), $h[p]$ $0 \le p \le P-1$ is the base-band equivalent CIR with P taps where $P < N_g$, and $w[n]$ represents the n^{th} additive white Gaussian noise (AWGN) sample. We assume that the CFO f is distributed as $f \sim \mathcal{U}[-f_{\max}, f_{\max}]$, where $\mathcal{U}[\cdot]$ represents the uniform distribution, and $f_{\max}$ is the maximum absolute value of the CFO. The CIR is distributed as $h[p] \sim \mathcal{CN}(0, \sigma_p^2)$, where $\mathcal{CN}(\cdot)$ represents the complex Gaussian distribution, and σ_p^2 is the power of the p^{th} path. Similarly, AWGN samples are distributed as $w[n] \sim \mathcal{CN}(0, \sigma_w^2) \forall n$. We assume that different channel taps and AWGN samples are uncorrelated.

Timing and frequency synchronization provide TO and CFO estimates, denoted as $\hat{d}$ and $\hat{f}$, respectively. We employ the first ZC sequence in (1) for signal detection and coarse TO estimation, after which both ZC sequences are employed for CFO estimation and TO estimate refinement.

III. Timing Synchronization Using ZC Sequence

For timing synchronization, a cross-correlation of the received signal with the local copy of the training sequence can be used. In this section, we analyze cross-correlation-based timing synchronization using a generic ZC sequence with a CP and CS and its sensitivity to CFOs. The cross-correlation of the received signal in (2) with a local copy of the ZC sequence is given as

$$\begin{aligned} r[l] &= \frac{1}{N}\sum_{n=0}^{N-1} y[n+l]e^{-j\frac{\pi}{N}un^2} \\ &= \frac{1}{N}\sum_{n=0}^{N-1} e^{j\frac{2\pi}{N}f(n+l)} \sum_{p=0}^{P-1} h[p]x[n+l-d-p]e^{-j\frac{\pi}{N}un^2} \\ &\quad + \frac{1}{N}\sum_{n=0}^{N-1} w[n+l]e^{-j\frac{\pi}{N}un^2}, \end{aligned} \tag{3}$$

where l is the lag of the cross-correlation. Note that, because of CP and CS, linear cross-correlation in (3) is similar to circular cross-correlation for $d \le l \le d + 2N_g - 1$. We denote this set of sample range as the circular-correlation region, $\mathcal{R}_{cc} \equiv \{l \in [d, d+2N_g-1]\}$. For a channel with P taps, the ISI-free region is $l \in [d+P-1, d+2N_g-1]$, as shown in Fig. 1, and the circular-correlation region encloses the ISI-free region. If the transmitted ZC sequence is $e^{j\frac{\pi}{N}un^2}, 0 \le n \le N_t - 1$, the l^{th} element of cross-correlation within $\mathcal{R}_{cc}$ is given as

$$\begin{aligned} r[l] &= \frac{1}{N}e^{j\frac{2\pi}{N}fl}\sum_{p=0}^{P-1} h[p] \sum_{n=0}^{N-1} e^{j\frac{2\pi}{N}fn} e^{j\frac{\pi}{N}u(n+l-d-N_g-p)^2} \\ &\quad \times e^{-j\frac{\pi}{N}un^2} + \frac{1}{N}\sum_{n=0}^{N-1} w[n+l]e^{-j\frac{\pi}{N}un^2} \\ &= \frac{1}{N}e^{j\frac{2\pi}{N}fl}\sum_{p=0}^{P-1} h[p]e^{j\frac{\pi}{N}u(l-d-N_g-p)^2} \\ &\quad \times \left(\sum_{n=0}^{N-1} e^{j\frac{2\pi}{N}\left(u(l-d-N_g-p)+f\right)n}\right) \\ &\quad + \frac{1}{N}\sum_{n=0}^{N-1} w[n+l]e^{-j\frac{\pi}{N}un^2},\ l \in \mathcal{R}_{cc}. \end{aligned} \tag{4}$$

In the absence of CFO, i.e., $f = 0$, the inner sum in (4) is non-zero only when $l = d + N_g + p$, $0 \le p \le P-1$. Hence, the cross-correlation term in (4) simplifies to

$$\begin{aligned} r[l] &= \sum_{p=0}^{P-1} h[p]\delta[l-d-N_g-p] \\ &\quad + \frac{1}{N}\sum_{n=0}^{N-1} w[n+l]e^{-j\frac{\pi}{N}un^2}, \quad \text{for } f = 0, \end{aligned} \tag{5}$$

with $\delta[l]$ being the Kronecker delta function. Note that (5) generates an estimate of the CIR for the set of indices $d + N_g \le l \le d + N_g + P - 1$, with the first tap $h[0]$ appearing at the correct starting index, i.e., $d + N_g$. The rest of the cross-correlation values within $\mathcal{R}_{cc}$ contain only noise. We denote the set of indices providing the CIR estimate as the "CIR region" given as

$$\mathcal{R}_{CIR} = \left\{ l \in [d+N_g, d+N_g+P-1] \right\} \subseteq \mathcal{R}_{cc}, \text{if } f = 0. \tag{6}$$

As the CIR region, in the absence of CFO, is a subset of the ISI-free region, peak detection corresponding to the strongest channel tap can be used for coarse TO estimation [20]. The CIR region is also used for channel estimation and fine TO estimation in [17], [18], which assume that coarse timing synchronization and CFO compensation have already been performed. Thus, the receiver knows $\mathcal{R}_{cc}$, and the residual CFO is also minimal. Based on these assumptions, a threshold is derived in [17] to locate the first tap of the multi-path channel that provides fine TO estimate in addition to the channel estimate provided by the cross-correlation. However, for a non-zero CFO, the value of the inner sum in (4) is clearly dependent on the CFO and decreases from N to zero as CFO increases from zero to one for each $l \in \mathcal{R}_{CIR}$ in (6). In addition, each cross-correlation value becomes a weighted sum of the channel taps and no longer provides the CIR estimate. Therefore, the fine timing and the channel estimation algorithms in [17] cannot be applied in this case. This dependency on CFO implies that cross-correlation-based coarse timing synchronization using ZC sequence or any general CAZAC sequence is sensitive to large CFOs. Thus, the goal of this paper is twofold: to identify ZC sequences, which offer robustness to CFOs and to design signal detection, TO and CFO estimation procedures using such sequences.

IV. ZC Sequence Design for CFO Robustness

In this section, we discuss how to design ZC sequences for the proposed training block in (1) to achieve robustness to CFOs. Using proposed robust sequences, we will then design the detection and synchronization algorithms in the following sections. We denote the cross-correlation of the received training block with the first ZC sequence in (1) as $r_1[l]$. Within the circular-correlation region, the cross-correlation term is

$$\begin{aligned} r_1[l] &= \frac{1}{N}e^{j\frac{2\pi}{N}fl}\sum_{p=0}^{P-1} h[p]e^{j\frac{\pi}{N}u(l-d-N_g-p)^2} \\ &\quad \times \left(\sum_{n=0}^{N-1} e^{j\frac{2\pi}{N}\left(u(l-d-N_g-p)+f\right)n}\right) \\ &\quad + \frac{1}{N}\sum_{n=0}^{N-1} w[n+l]e^{-j\frac{\pi}{N}un^2},\ l \in \mathcal{R}_{cc}, \end{aligned} \tag{7}$$

which is the same as (4).

A. Effect of Integer CFOs

Let us represent the CFO by the sum of an integer part f_{I} and a fractional part $-0.5 \leq f_{\mathrm{F}} \leq 0.5$ so that $f = f_{\mathrm{I}} + f_{\mathrm{F}}$. In this section, we assume that $f_{\mathrm{F}} = 0$ to concentrate on integer CFOs. Note that the sum within the parenthesis in (7) is non-zero only when

$$u(l - d - N_{\mathrm{g}} - p) + f_{\mathrm{I}} = mN, \tag{8}$$

where m is any integer and $l \in \mathcal{R}_{\mathrm{cc}}$. For $f_{\mathrm{I}} = 0$, the condition in (8) is satisfied whenever $l = d + N_{\mathrm{g}} + p$, for any $0 \leq p \leq P-1$ with $m = 0$ and $r_1[l]$ reduces to (5) and $\mathcal{R}_{\mathrm{CIR}}$ is the same as in (6). However, it is important to note that when $|f_{\mathrm{I}}|$ is a non-zero integer value, the condition in (8) will be satisfied for different values of lag l within the circular-correlation region, or it may not be satisfied at all. Hence, the indices or the values of lag l in $\mathcal{R}_{\mathrm{CIR}}$ will change and shift away from the ideal location in (6) for non-zero integer CFOs. The amount of shift depends on the values of N, u, and f_{I}. For example, with $N = 256$, $N_{\mathrm{g}} = 16$, $P = 12$, $f_{\mathrm{I}} = 1$, and $u = 85$, (8) is satisfied for $m = 1$ and $l = d + N_g + p + 3$ with $\mathcal{R}_{\mathrm{CIR}} = [d + N_{\mathrm{g}} + 3, d + N_{\mathrm{g}} + 3 + P - 1]$, resulting in a shift of three samples in the CIR region, which still lies within the ISI-free region. In contrast, for $u = 17$ and $f_{\mathrm{I}} = 2$, (8) is satisfied for $m = 2$ and $l = d + N_g + p + 30$ with $\mathcal{R}_{\mathrm{CIR}} = [d + N_{\mathrm{g}} + 30, d + N_{\mathrm{g}} + 30 + P - 1]$, which is no longer within the ISI-free region. Hence, because of the shift in the CIR region in the presence of integer CFOs, the value of the root index can significantly affect the performance of TO estimation. The following two propositions show that the CIR region shifts linearly with CFO, and the elements in CIR region are unique.

Proposition 1: Let l_i denote the index of the CIR region corresponding to $h[0]$, for $f_{\mathrm{I}} = i$, where i is an integer. If there exists l_1 such that $u(l_1 - N_g - d) + 1 = m_1 N$, then $l_{i+1} = l_i + (l_1 - N_g - d)$ satisfies $u(l_{i+1} - N_g - d) + i + 1 = m_{i+1} N$ with $m_{i+1} = (i+1)m_1$.

Proof: See Appendix A. A similar proposition shows that $l_{i-1} = l_i - (l_1 - N_g - d)$.

Proposition 2: The indices of $\mathcal{R}_{\mathrm{CIR}}$ within $\mathcal{R}_{\mathrm{cc}}$ are unique given $N_{\mathrm{g}} < \frac{N}{2}$.

Proof: See Appendix B.

Proposition 1 implies that, given u, N, N_{g}, and f_{I}, each element in $\mathcal{R}_{\mathrm{CIR}}$ shifts linearly by $s = l_1 - N_{\mathrm{g}} - d$ samples with a unit shift in f_{I}, and the value of s depends on the value of the root index u for a given N. Hence, for $f = f_{\mathrm{I}}$, $r_1[l]$ becomes

$$r_1[l] = e^{j\frac{2\pi}{N} f_{\mathrm{I}} l} \sum_{p=0}^{P-1} h[p]\delta(l - d - N_g - p - s f_{\mathrm{I}}) + \frac{1}{N} \sum_{n=0}^{N-1} w[n+l] e^{-j\frac{\pi}{N} u n^2}, \qquad \forall\, l \in \mathcal{R}_{\mathrm{cc}}. \tag{9}$$

Proposition 1 also implies that if f_{I} keeps on increasing, $\mathcal{R}_{\mathrm{CIR}}$ will eventually move out of $\mathcal{R}_{\mathrm{cc}}$, and if $l_{i\pm1} = l_i \pm (l_1 - N_g - d) \gtrless N$, then $(l_{i\pm1})_N$ satisfies (8), where $(\cdot)_N$ represents the modulo N operation. This implies that the shift in CIR region is eventually periodic. However, outside $\mathcal{R}_{\mathrm{cc}}$, linear correlation is no longer equal to circular correlation. Moreover, in OFDM systems, the TO estimate must belong to the ISI-free region, which is in turn a subset of $\mathcal{R}_{\mathrm{cc}}$. As coarse TO will be estimated using cross-correlation values in the CIR region, whose location is unknown because integer CFO is unknown (CFO estimation is performed after coarse timing synchronization), it implies that the TO estimate also shifts left or right from the correct location by s samples with each unit increase or decrease in the integer CFO, respectively. If $f_{\max}$ is the maximum absolute integer CFO that can be observed in the system, $\mathcal{R}_{\mathrm{CIR}}$ will be a subset of $[d + N_g - s f_{\max}, d + N_g + s f_{\max} + P - 1]$. If the CIR region is restricted within the ISI-free region for $f \leq f_{\max}$, the TO estimate will also be within ISI-free region, which motivates the design of the proposed preamble. We introduce the CS along with the CP, which extends the circular-correlation region and allows the CIR region to shift in eithe direction and still remain within the ISI-free region for a certain maximum CFO given as

$$f_{\max} = \left| \left\lfloor \frac{N_{\mathrm{g}} - (P-1)}{s} \right\rfloor \right|. \tag{10}$$

B. Choosing the Root Index

As the root index determines the amount of shift s in the CIR region for a unit change in CFO, it is important to select a root index which results in the minimum possible value of s, for it will maximize $f_{\max}$ in (10) that the coarse timing synchronization can handle. A smaller value of s also helps in training block detection, discussed in Section V. Hence, we choose a root index that is relative prime to N based on the definition of ZC sequence and satisfies

$$u(l_1 - N_g - d) = us = m_1 N - f_{\mathrm{I}} \tag{11}$$

for $f_{\mathrm{I}} = 1$ or -1 with the minimum possible s. An obvious choice is $u = \pm 1$ or $\pm(N-1)$, which results in the minimum possible $s = \mp 1$. Otherwise, any factor of $m_1 N \pm 1$ that is relative prime to N can be used as u. For example, if N is an even number not divisible by 3 (N is usually a power of 2 in OFDM systems), one of $m_1 N \pm 1$ must be divisible by $s = 3$, which provides the second minimum value of s for any even N. As an example, for $N = 256$, $N_g = 32$ and $P = 17$, $u = 1$ gives $s = -1$ and the TO estimate remains in the ISI-free region for $f_{\max} = 16$. For the same parameters, $u = 85$ gives $s = 3$ and $f_{\max} = 5$, while $u = 51$ gives $s = 5$ and $f_{\max} = 3$. As the length of CP in OFDM systems is always longer than the maximum excess delay of the channel, and $f_{\max}$ in practical systems is usually 1 or 2, a number of choices for root indices can be employed for specific values of N, N_{g}, and $f_{\max}$. For example, for the LTE-DL system parameters for 20 MHz transmission with extended cyclic prefix, $N = 2048$, and $N_g = 512$. A typical clock accuracy of 10 ppm results in $f_{\max} = 2$, and ITU vehicular-A channel [30], as an example, has $P = 77$. For these practical system parameters, a number of feasible root indices exist including $u = \pm 1, \pm 91, \pm 273, \pm 315, \pm 585, \pm 455$, and ± 1365.[1]

[1]The definition of root indices for ZC sequences defined in the sub-carrier domain is discussed in Section IV-C.

TABLE I
SHIFTS IN CROSS-CORRELATION MAXIMA WITH INTEGER CFOS FOR ROOT INDICES OF LTE DOWNLINK PSS

root index (u_f)	$(f=-2)$	$(f=-1)$	$(f=0)$	$(f=1)$	$(f=2)$
25	423	−813	0	813	−423
29	−163	−943	0	943	−163
34	163	943	0	−943	163

C. Choosing the Root Indices for ZC Sequences Defined in the Sub-Carrier Domain

The proposed training block in (1) contains ZC sequences defined in the time domain. However, a training block can also be defined by modulating certain sub-carriers of an OFDM symbol with a ZC sequence. For example, in LTE DL, primary synchronization signal (PSS) contains ZC sequences, defined only for the middle 63 sub-carriers of the OFDM symbol. In this section, we discuss the design of root indices for ZC sequences for such training symbols. We derive a condition similar to (11) that can help the designer to choose root indices that minimize the shift s in the cross-correlation for integer CFOs. Please note that the synchronization algorithms proposed in the following sections are still based on the training signal in (1).

Let us consider an OFDM training symbol with a ZC sequence centered around DC sub-carrier occupying a subset of M sub-carriers out of N total sub-carriers, and given as

$$X[k]=e^{j\frac{\pi}{M}u_f k(k+1)},\quad k\in\mathcal{I}:=\{-(M-1)/2,\cdots,(M-1)2\}\setminus\{0\}, \tag{12}$$

for odd M and

$$X[k]=e^{j\frac{\pi}{M}u_f k^2},\ k\in\mathcal{I}:=\{-M/2,\ \cdots,\ M/2-1\}\setminus\{0\}, \tag{13}$$

for even M, where k is the sub-carrier index, u_f is the root-index of the ZC sequence defined in the sub-carrier domain, and $\mathcal{I}$ is the set of sub-carriers modulated by the ZC sequence. The rest of the sub-carriers are zero.[2] As an example, in LTE DL transmissions $M=63$. An IDFT (inverse discrete Fourier transform) of the training symbol followed by CP and CS insertions result in the training signal

$$x[n]=\sum_{k=-\frac{N}{2}}^{\frac{N}{2}-1}X[k]e^{j\frac{2\pi}{N}k(n-N_g)},\quad 0\leqslant n\leqslant N_t-1. \tag{14}$$

The received signal is given as in (2). The cross-correlation is then given as

$$r[l]=\frac{1}{N}\sum_{n=0}^{N-1}y[n+l]x^*[n+N_g], \tag{15}$$

and the circular correlation region is still defined as $\mathcal{R}_{\text{cc}}=\{d\leq l\leq d+2N_g-1\}$. We use the fact that the N-point circular correlation of two sequences in the time domain is equivalent to the point-by-point multiplication in the frequency domain of the N point DFT of one sequence and the conjugate of the DFT of the other sequence. As the N point DFT of $y[n]$, $d+N_g\leq n\leq d+N_g+N-1$, for an integer CFO f_{I} is given as

$$Y[k]=\begin{cases}e^{-j\frac{2\pi}{N}k(d+N_g)}H[k-f_{\text{I}}]X[k-f_{\text{I}}] & k\in\mathcal{I},\\ 0 & \text{otherwise,}\end{cases} \tag{16}$$

where $H[k]$ is the N point DFT of the CIR $h[p], 0\leq p\leq P-1$, the cross-correlation in (15) for $l\in\mathcal{R}_{\text{cc}}$ can be equivalently expressed as

$$r[l]=\frac{1}{N}\sum_{k=-\frac{N}{2}}^{\frac{N}{2}-1}e^{-j\frac{2\pi}{N}k(d+N_g)}H[k-f_{\text{I}}]X[k-f_{\text{I}}]X^*[k]e^{j\frac{2\pi}{N}kl}+\frac{1}{N}\sum_{n=0}^{N-1}w[n]x^*[n],\qquad\forall l\in\mathcal{R}_{\text{cc}}. \tag{17}$$

Using the definition of the training symbol in (13), the product $X[k-f_{\text{I}}]X^*[k]$ is non-zero for $k\in\mathcal{I}':=[\frac{-M}{2}+f_{\text{I}},\ldots,-1,f_{\text{I}}+1,\ldots,\frac{M}{2}-1]$ for a positive f_{I}, and $\mathcal{I}':=[\frac{-M}{2},\ldots,f_{\text{I}}-1,1,\ldots,\frac{M}{2}-1]$ for a negative f_{I}. Hence,

$$r[l]=\frac{1}{N}e^{j\frac{\pi}{M}u_f f_{\text{I}}^2}\sum_{p=0}^{P-1}h[p]e^{j\frac{2\pi}{N}f_{\text{I}}p}\times\left(\sum_{k\in\mathcal{I}'}e^{j\frac{2\pi}{N}(l-d-N_g-p-\frac{N}{M}u_f f_{\text{I}})k}\right)+\frac{1}{N}\sum_{n=0}^{N-1}w[n]x^*[n]. \tag{18}$$

The term inside the parentheses is maximum (equal to $|\mathcal{I}'|$) whenever lag l satisfies

$$l-d-N_g-p-\frac{N}{M}u_f f_{\text{I}}=mN \tag{19}$$

where m is any integer. The training sequence with odd M in (12) also results in the same condition. This condition is in fact similar to the condition in (11) (with $p=0$ except that N is replaced by $\frac{N}{M}$), and it can be used to predict the shift in the cross-correlation peak with integer CFOs. Unlike (9), the cross-correlation in (18) does not yield the CIR when $M<N$. However, the peak or energy detection can still be used for training block detection and coarse timing synchronization for appropriately chosen root indices. Analyzing (19), $u_f=\pm1$ again results in the minimum value of the shift $s=1$. However, as $\frac{N}{M}$ may not be an integer, the value of s may not be exactly an integer for an integer CFO. Viewed in another way, to get an integer s, the value of CFO may not be exactly an integer. For example, in one of the LTE PSSs, $N=2048$, $M=63$, and $u_f=25$ result in $s=812.69\approx 813$ samples for $f=1$, or $s=813$ samples for $f=1.004\approx 1$. Table I shows the values of shifts obtained for $f=1$ and 2 in all three LTE PSSs. As obvious, none of the root indices have s that lies in ISI-free region for $f=1$. Hence, cross-correlation-based

[2]If the training symbol also contains data sub-carriers as in PSS, low-pass filtering can be performed prior to cross-correlation to reject the contribution of data sub-carriers on the cross-correlation.

synchronization is not feasible for LTE in the presence of integer CFOs without further modifications. Thus, blind coarse-timing synchronization, as opposed to cross-correlation-based timing synchronization, is usually proposed for LTE downlink, as in [31].

V. Detection and Coarse Timing Offset Estimation With Unknown CFO

The previous section described the effect of integer CFOs on timing synchronization and presented conditions to select the appropriate root indices of the ZC sequences to achieve robustness to integer CFOs. However, the effect of fractional CFO was neglected for simplification. We observed that integer CFOs do not affect the values of the cross-correlation but result only in a translation of these values. Therefore, from a perspective of fractional CFOs, zero or non-zero integer CFOs are the same, and the analysis for fractional CFOs with zero integer CFO can be directly applied to the case of non-zero integer CFOs for the corresponding shifted samples.

In this section, we develop training block detection and coarse timing synchronization schemes using the ZC sequences with proposed root indices. Note that, for detection and coarse timing synchronization, only the first ZC sequence in the training block in (1) is employed. Also, f_{F} is no longer zero so that $|f| \leq f_{\max}$ is a real number. Equation (7) can then be written as

$$\begin{aligned} r_1[l] &= e^{j\frac{\pi}{N}(2l+N-1)f} e^{j\frac{\pi}{N}u((l-d-N_g)^2+(N-1)(l-d-N_g))} \\ &\quad \times \sum_{p=0}^{P-1} h[p] e^{j\frac{\pi}{N}u\left(p^2-\{2(l-d-N_g)+N-1\}p\right)} \\ &\quad \times \Psi\left(u\{p-(l-d-N_g)\}\right) + \frac{1}{N}\sum_{n=0}^{N-1} w[n+l] e^{-j\frac{\pi}{N}un^2}, \\ &\quad \forall l \in \mathcal{R}_{\mathrm{cc}}, \end{aligned} \tag{20}$$

where

$$\Psi\left(u\{p-(l-d-N_g)\}\right) = \frac{1}{N}\frac{\sin\pi\left(u\left(p-(l-d-N_g)\right)-f\right)}{\sin\frac{\pi}{N}\left(u\left(p-(l-d-N_g)\right)-f\right)}.$$

As each channel tap $h[p] \sim \mathcal{CN}(0,\sigma_p^2)$, and different taps of the channel and noise samples are assumed to be uncorrelated, the cross-correlation values are distributed as follows:

$$r_1[l] \sim \mathcal{CN}\left(0, \sum_{p=0}^{P-1} \sigma_p^2 \Psi^2\left(u\{p-(l-d-N_g)\}\right) + \sigma_{\tilde{w}}^2\right), \tag{21}$$

for each $l \in \mathcal{R}_{\mathrm{cc}}$, given s and f, where $\sigma_{\tilde{w}}^2 = \frac{\sigma_w^2}{N}$. $\Psi^2(x)$ is a square of the periodic sinc function whose magnitude is maximum (equal to 1) in the center of its main lobe ($|x| \leq 1$) and decreases rapidly as we move away from the main lobe when $|x|$ increases. As p varies, different samples of $\Psi^2(u\{p-(l-d-N_g)\})$ contribute to the summation in (21). These samples have significant magnitude only for those values of p that satisfy $p-(l-d-N_g) = ms$, where m is any integer

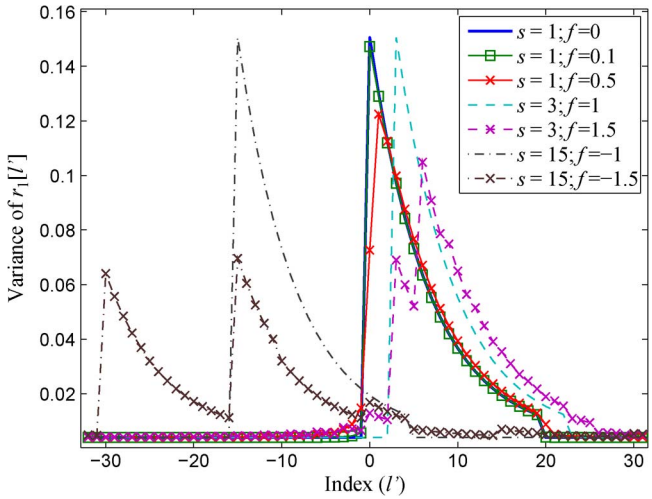

Fig. 2. Variance of $r_1[l']$ with different values of s and f; $N=256$, $N_{\mathrm{g}}=32$, $P=20$.

because $ums = mm_1N - m$, and a sample close to the main lobe of $\Psi^2(u\{p-(l-d-N_g)\})$ is obtained. In that case,

$$\Psi^2\left(u\{p-(l-d-N_g)\}\right) = \frac{\sin^2(\pi f)}{\sin^2\frac{\pi}{N}(m+f)} \approx \frac{N^2\sin^2(\pi f)}{\pi^2(m+f)^2},$$

where we use $\sin^2(x) \approx x^2$ for small x. Thus, neglecting the samples far from the main lobe and applying some algebraic manipulations, (20) and (21) can be approximated as

$$\begin{aligned} r_1[l'] &\approx \frac{\sin(\pi f)}{\pi} e^{j\frac{\pi}{N}(2l+N-1)f} \sum_{m=-\lfloor\frac{l'}{s}\rfloor}^{\lfloor\frac{P-1-l'}{s}\rfloor} h[ms+l'] \\ &\quad \times e^{-j\frac{\pi}{N}(m^2s+m)} \frac{1}{(m+f)} \\ &\quad + \frac{1}{N}\sum_{n=0}^{N-1} w[n+l'+d+N_g] e^{-j\frac{\pi}{N}un^2}, \end{aligned} \tag{22}$$

for $0 \leq l' = l-d-N_g \leq P-1$, and

$$r_1[l'] \sim \mathcal{CN}\left(0, \frac{\sin^2(\pi f)}{\pi^2} \sum_{m=-\lfloor\frac{l'}{s}\rfloor}^{\lfloor\frac{P-1-l'}{s}\rfloor} \sigma_{ms+l'}^2 \frac{1}{(m+f)^2} + \sigma_{\tilde{w}}^2\right). \tag{23}$$

We see that in the presence of fractional CFOs, the cross-correlation no longer provides channel estimates, for each cross-correlation value within $\mathcal{R}_{\mathrm{cc}}$ is a weighted sum of the CIR. As an illustration, Fig. 2 shows the change in the variance of $r_1[l']$ in (23) for an exponential power delay profile (PDP), with $N=256$, $N_{\mathrm{g}}=32$, $P=20$, and different values of CFO and shift s corresponding to different root indices. As shown, $f=0$ provides the actual PDP of the channel starting at $l'=0$, while it shifts by 3 and -15 samples for $f=1$ and $f=-1$ with $s=3$ and $s=15$, respectively, while the values remain the same. However, as f_{F} changes, the change in the variance depends on f_{F} itself as well as the values of s. As f changes from an integer i to $i+1$, the PDP obtained at $l' \in [is : is+P-1]$ begins to decrease while its copy at $l' \in [(i+1)s : (i+1)s+P-1]$ begins to increase until the former disappears completely at $f=i+1$. For any intermediate value between i to $i+1$, the

resultant variance of the cross-correlation is given by (23). If $s \ll P$, the resultant variance is still concentrated in a region $[is : (i+1)s + P - 1]$, as shown in Fig. 2 for $s = 1$ and 3. However, if s is comparable to P, two copies remain distinct because of a higher value of s, and the effective PDP expands, as shown in the case of $s = 15$.

Moreover, (22) shows that the correlation between $r_1[l'], \ldots, r_1[l' + s - 1]$ is very small (less than $\sigma_{\tilde{w}}^2$) as it is only due to noise samples and $\sigma_w^2 \ll N$ for practical signal-to-noise ratios (SNR). We define the SNR as $\frac{\sum_{p=0}^{P-1}\sigma_p^2}{\sigma_w^2}$. The correlation between $r_1[l']$ and $r_1[l' \pm is]$ is given as

$$\sigma_{r_1[l'],r_1[l'\pm is]} = \frac{\sin^2(\pi f)}{\pi^2} e^{j\frac{2\pi}{N} isf} \times \sum_{m=\lfloor -\frac{l'}{s} \rfloor}^{\lfloor \frac{P-1-l'}{s} \rfloor} \sigma_{ms+l'}^2 \frac{1}{(m+f)(m\mp i+f)}. \quad (24)$$

As expected, when f is an integer, the correlation in (24) is zero and increases as $|f_{\mathrm{F}}|$ increases from 0 to 0.5. However, as the factor $\frac{1}{(m\pm f)(m\mp i\pm f)}$ decreases exponentially with m, the correlation is still very small particularly for exponential PDPs and small values of s. Hence, as an approximation to simplify the synchronization and detection schemes, we assume that cross-correlation samples are uncorrelated.

A. Neyman-Pearson Detection

After gaining insights into the distribution of cross-correlation, we now focus on the design of training block detection and coarse timing synchronization algorithms. To distinguish the presence or absence of a training block, we also need the distribution of cross-correlation outside the circular-correlation region. We assume that the training sequence is transmitted as a preamble and the received signal before the training block contains only noise samples. Assuming that the noise samples are uncorrelated, the distribution of the cross-correlation is

$$r_1[l'] \sim \mathcal{CN}\left(0, \sigma_{\tilde{w}}^2\right), \quad l' < 0. \quad (25)$$

To find a criterion for determining whether the cross-correlation values come from a received training symbol or only noise samples, we use the Neyman-Pearson (NP) test [32]. Instead of processing each output sample of the cross-correlation individually, we process a window of cross-correlation samples to take all the samples of cross-correlation, corresponding to the CIR region, into account simultaneously. We also assume that $s \ll P$ so that the extension in the CIR region due to fractional CFOs is minimal. The test evaluates the absolute values in a window of last P samples of the cross-correlation $\mathbf{r}[l] = [|r_1[l-(P-1)]|, \ldots, |r_1[l]|]^T$ to declare in favor of the null or the alternative hypothesis defined as

Null Hypothesis (H_o):

$$\mathbf{r}[l] \sim \left(\frac{2}{\sigma_{\tilde{w}}^2}\right)^P \exp\left(-\frac{1}{\sigma_{\tilde{w}}^2}\sum_{k=0}^{P-1}|r_1[l+k-(P-1)]|^2\right) \times \prod_{k=0}^{P-1}|r_1[l+k-(P-1)]|, \quad (26)$$

Alternate Hypothesis (H_a):

$$\mathbf{r}[l] \sim \exp\left(-\sum_{k=0}^{P-1}\frac{1}{\sigma_k^2}|r_1[l+k-(P-1)]|^2\right) \times \prod_{k=0}^{P-1}\left(\frac{2}{\sigma_k^2}|r_1[l+k-(P-1)]|\right), \quad (27)$$

with

$$\sigma_k^2 = \frac{\sin^2(\pi f)}{\pi^2}\sum_{m=-\lfloor \frac{k}{s} \rfloor}^{\lfloor \frac{P-1-k}{s} \rfloor}\sigma_{ms+k}^2\frac{1}{(m+f)^2} + \sigma_{\tilde{w}}^2, \quad (28)$$

where we use the fact that the absolute value of a complex Gaussian random variable has Rayleigh distribution. In addition, we assume that the cross-correlation values are uncorrelated in the cross-correlation region as discussed in the previous section. Through simulations in Section VII, we will demonstrate that the effect of this independence assumption is minimal. Based on the null and alternative hypotheses, the NP test is given as

Decide H_a if

$$\frac{\Pr[\mathbf{r}[l];H_a]}{\Pr[\mathbf{r}[l];H_o]} = \frac{\left(\sigma_{\tilde{w}}^2\right)^P}{\prod_{k=0}^{P-1}\sigma_k^2} \times \exp\left(-\sum_{k=0}^{P-1}|r_1[l+k-(P-1)]|^2\left(\frac{1}{\sigma_k^2}-\frac{1}{\sigma_{\tilde{w}}^2}\right)\right) > \gamma, \quad (29)$$

where γ is the threshold. Equation (29) is equivalent to

$$\frac{1}{P}\sum_{k=0}^{P-1}\frac{\sigma_k^2-\sigma_{\tilde{w}}^2}{\sigma_k^2\sigma_{\tilde{w}}^2}|r_1[l+k-(P-1)]|^2 > \gamma' \quad (30)$$

where γ' is the value satisfying

$$\Pr\left[\frac{1}{P}\sum_{k=0}^{P-1}\frac{\sigma_k^2-\sigma_{\tilde{w}}^2}{\sigma_k^2\sigma_{\tilde{w}}^2}|r_1[l+k-(P-1)]|^2 > \gamma'\right] = P_{\mathrm{FA}} \quad (31)$$

under H_o for a target probability of false alarm P_{FA}. Under H_o, $\frac{1}{P}\frac{\sigma_k^2-\sigma_{\tilde{w}}^2}{\sigma_k^2\sigma_{\tilde{w}}^2}|r_1[l+k-(P-1)]|^2$ for each $k \in [0, P-1]$ has exponential distribution with rate $\lambda_k = \frac{P\sigma_k^2}{\sigma_k^2-\sigma_{\tilde{w}}^2}$. Therefore, $\frac{1}{P}\sum_{k=0}^{P-1}\frac{\sigma_k^2-\sigma_{\tilde{w}}^2}{\sigma_k^2\sigma_{\tilde{w}}^2}|r_1[l+k-(P-1)]|^2$ has the hypo-exponential distribution [33, p. 308] and

$$\Pr\left[\frac{1}{P}\sum_{k=0}^{P-1}\frac{\sigma_k^2-\sigma_{\tilde{w}}^2}{\sigma_k^2\sigma_{\tilde{w}}^2}|r_1[l+k-(P-1)]|^2 > \gamma'\right] = \sum_{k=0}^{P-1}C_{k,P}\exp(-\gamma'\lambda_k), \quad (32)$$

where

$$C_{k,P} = \prod_{\substack{m=0,1,\ldots,P-1 \\ m\neq k}}\frac{\lambda_m}{\lambda_m-\lambda_k}. \quad (33)$$

Hence, the test for signal detection calculates a running weighted power estimate of the cross-correlation according to (30), and if the estimate is greater than γ', it declares the detection of the training block. The corresponding index is then taken as the coarse TO estimate $\hat{d}$. Thus,

$$\hat{d} = l - P + 1 : \frac{1}{P}\sum_{k=0}^{P-1} \frac{\sigma_k^2 - \sigma_{\tilde{w}}^2}{\sigma_k^2 \sigma_{\tilde{w}}^2} \left| r_1 \left[l + k - (P-1) \right] \right|^2 > \gamma'. \quad (34)$$

However, in some cases, the condition in (34) can be triggered early due to a partial correlation with the CP of the training signal for $l = d + N_g - N$. To avoid a wrong TO estimate in that case, the algorithm picks the index of the maximum value of the power estimate in (34) out of the $N + N_g$ indices following the index for which the condition in (34) is satisfied. From (30) and (31), it is clear that both the test criterion and the calculation of γ' require knowledge of the channel PDP and the $\sigma_{\tilde{w}}^2$. In addition, the calculation of σ_k^2 in (28) also requires the values of CFO. We now derive an approximation that can alleviate some of these requirements.

1) Simplified Neyman-Pearson Detection: For high values of SNR and/or large N, $\sigma_{\tilde{w}}^2 \ll \sigma_k^2$. Moreover, channel taps below the noise floor of the system cannot be estimated. Therefore, $\lim_{\mathrm{SNR}\to\infty} \lambda_k = \lim_{\mathrm{N}\to\infty} \lambda_k = P$, and the asymptotic distribution of the weighted windowed energy in (30) approaches the Erlang distribution with rate P. Using this approximation, (32) simplifies to

$$\Pr\left[\frac{1}{P}\sum_{k=0}^{P-1} \frac{\sigma_k^2 - \sigma_{\tilde{w}}^2}{\sigma_k^2 \sigma_{\tilde{w}}^2} \left| r_1 \left[l + k - (P-1) \right] \right|^2 > \gamma' \right] = \sum_{k=0}^{P-1} \frac{1}{k!} \exp\left(-P\gamma'\right) \left(P\gamma'\right)^k. \quad (35)$$

Similarly, the test criterion in (30) can be approximated as

$$\frac{1}{P}\sum_{k=0}^{P-1} \frac{1}{\sigma_{\tilde{w}}^2} \left| r_1 \left[l + k - (P-1) \right] \right|^2 > \gamma'. \quad (36)$$

Note that neither the test criterion nor the calculation of γ' for this approximation depend on the channel PDP or CFO. However, the test still requires an estimate of the noise variance [34], which is also required for fine TO estimation in [17]. The value of P can be calculated through the delay spread of the channel. We will evaluate the robustness of this simplified NP detection and compare its performance with the original detection test in (30) in Section VII.

This simplified NP detection completes the discussion of training block detection and coarse timing synchronization. We have investigated the effect of integer CFOs on cross-correlation-based timing synchronization using ZC sequences and shown that given system parameters, some ZC sequences can minimize the shift in the CIR region as the CFO increases. A smaller value of s also helps to maintain the channel profile within the CIR region and allows us to design a test used for both signal detection and coarse TO estimation. A simplified detection test criterion also alleviates the constraints of *a priori* information about channel PDP and CFO. Thus, the proposed cross-correlation-based detection and coarse timing synchronization schemes are robust to CFOs as these schemes do not requiring the knowledge of CFOs. Once the training block is detected and correspondingly, a coarse TO estimate is available, the receiver can proceed to CFO estimation, discussed in the following section.

Remark 1: (Noise variance estimation) The simplified NP test in (36) requires an estimate of the effective noise variance $\sigma_{\tilde{\omega}}^2$ for which noise estimation methods proposed in the literature like [34] can be employed. Although, proposing a new noise variance estimation method is beyond the scope of this paper, we present a simple scheme for noise variance estimation. As the proposed training block is transmitted as a preamble, the received signal before the preamble contains only noise. Therefore, we use a running power estimate of the received signal samples for noise variance estimation. Specifically, if the cross-correlation for lag l is computed as in (3), $\sigma_{\tilde{\omega}}^2$ used for detection employing $r[l]$, is estimated as,

$$\hat{\sigma}_{\tilde{\omega}}^2[l] = \frac{1}{MN}\sum_{n=0}^{M-1} \left| y[l - n - 2N_g] \right|^2 \quad (37)$$

where M is the number of samples used for noise-variance estimation. A lag of $2N_g$ samples ensures that $\sigma_{\tilde{\omega}}^2$ estimate in (37) employs only noise samples for $l \in \mathcal{R}_{cc}$. The accuracy of noise variance estimate will degrade (larger than the actual value) as the cross-correlation moves further along samples ($l > d + 2N_g$) but it actually helps in reducing false alarms according to (36) as the noise variance estimate will be larger than the actual value. We show the effect of noise variance estimation on the performance of simplified NP test in Section VII.

Remark 2: (Midamble detection): A training block can also be transmitted as a midamble, which refers to a training block with at least one data symbol before and after it. For example, in LTE DL with the extended-CP mode, a training block is transmitted in the sixth OFDM symbol of each half-frame containing sixty OFDM symbols. We discuss how the proposed training block detection and coarse timing synchronization scheme can be adapted for midamble detection. We assume, as in the case of cellular communications, that a continuous stream of signal is transmitted on the DL. Therefore, *noise only* hypothesis does not exist in this case; rather the *noise only* case is replaced by the *noise+random data* case. A false alarm now refers to a case in which a cross-correlation with the random data symbol preceding the training symbol is mistaken as the training symbol. However, assuming that the data symbols are uncorrelated from the training block, midamble detection can be performed as preamble detection with increased noise level. Assuming that the transmitted signal has unit power and the channel has unit average energy, the distribution of $r_1[l']$ under the null hypothesis is given as

$$r_1[l'] \sim \mathcal{CN}\left(0, \frac{\sigma_w^2 + \sum_{p=0}^{P-1} \sigma_p^2}{N}\right) = \mathcal{CN}\left(0, \frac{\sigma_w^2 + 1}{N}\right), \quad l' < 0, \quad (38)$$

as opposed to (25). The test criterion and the calculation of the threshold in (30) and (31), respectively, remain the same with

$\sigma^2_{\tilde{w}}$ replaced by $\frac{\sigma^2_w+1}{N}$. As the effective noise variance for the test criterion, that is, $\frac{\sigma^2_w+1}{N}$ does not approach zero with higher SNR values, the approximation in Section V-A1 is valid only for large values of N. However, an advantage of the frame-based continuous transmission is that the receiver can take advantage of the *a priori* information about periodicity of the midamble. Specifically, if the midamble is repeated once every S OFDM symbols, the receiver can perform peak detection on the running power estimate in (36) corresponding to all S symbols, followed by peak validation using the threshold γ'. Therefore, for midamble detection, the test in (36) can be modified as follows:Decide H_a if

$$\max\left(\frac{1}{P}\sum_{k=0}^{P-1}\frac{N}{\sigma^2_{\tilde{w}}+1}\left|r_1\left[l+k-(P-1)\right]\right|^2\right)>\gamma' \tag{39}$$

for $0 \le l \le NS$, and the TO estimate can be obtained from the index of the maximum value of the metric in (39). As the "*noise only*" hypothesis is replaced by the "*noise+random data*," the method for noise variance estimation outlined in *Remark* 1 can also be used for midamble detection.

VI. Carrier Frequency Offset Estimation

In this section, we discuss CFO estimation using the proposed training block. As CFO estimation requires an estimate of the symbol boundaries, the coarse TO estimate obtained through the NP test is employed for CFO estimation. Fractional CFO estimation is carried out first, followed by integer CFO estimation.

A. Fractional CFO Estimation

For fractional CFO estimation, we use correlation-based CFO estimation proposed in [23]. A blind CFO estimation scheme is proposed in [23] using a correlation of the CP of the received signal with its corresponding samples. As the first P samples of the CP are corrupted by the ISI, the CFO estimate is correct if the last $N_g - P$ samples of the CP are employed for CFO estimation. However, in the proposed training block, apart from the last $N_g - P$ samples of the CP, all the samples corresponding to the CS are also ISI-free for both the first and the second ZC sequence. Thus, we employ the CS and its corresponding samples of both ZC sequences for fractional CFO estimation. Specifically, the fractional CFO estimate can be obtained using (40) shown at the bottom of the page, where $\hat{d}$ is the coarse TO estimate obtained using the original (30) or simplified NP test (36). For a non-zero f_I, the coarse TO estimate can have an error of sf_I samples as compared to the ideal TO estimate, i.e., $d + N_g$. However, for the proposed root indices, $s \ll N_g$, and the effect of this shift can be neglected. Once $\hat{f}_{\text{frac}}$ is available, its effect can be removed from each received OFDM symbol as follows:

$$y_c[n] = e^{-j\frac{2\pi}{N}fn}y[n] \quad 0 \le n \le N_t - 1. \tag{41}$$

B. Integer CFO Estimation

After fractional CFO estimation and compensation, we employ both ZC sequences in the training block to estimate the integer CFO. As coarse TO estimate $\hat{d}$ is already available, the receiver has an estimate of the indices of the circular correlation regions corresponding to both ZC sequences in the training block. The receiver then calculates cross-correlations of the compensated training block with both ZC sequences given as

$$r_1[l] = \sum_{n=0}^{N-1} y_c[n+l]e^{-j\frac{\pi}{N}un^2},\ \hat{d}-N_g \le l \le \hat{d}+N_g-1, \tag{42}$$

and

$$r_2[l] = \sum_{n=0}^{N-1} y_c[n+l]e^{j\frac{\pi}{N}un^2},\ \hat{d}-N_g+N_t \le l \le \hat{d}+N_g+N_t-1, \tag{43}$$

for their respective circular correlation regions. As the fractional CFO has already been compensated for, both cross-correlations will provide an estimate of the CIR, but the locations of CIR regions will differ. As the second ZC sequence in the training block is the conjugate of the first sequence, the root index of the second ZC sequence is $-u$, instead of u for the first sequence. Therefore, if the CIR region for $r_1[l]$ is $\mathcal{R}_{\text{CIR},1} = [d+N_g+sf_I, d+N_g+sf_I+P-1]$, the CIR region for $r_2[l]$ will be $\mathcal{R}_{\text{CIR},2} = [d+N_g+N_t-sf_I, d+N_g+N_t-sf_I+P-1]$. The maximum distance between the CIR regions of $r_1[l]$ and $r_2[l]$ can be $2sf_{\max}$. As the location of CIR regions is dependent on f_I, the index for which the difference between the two cross-correlations is minimized can be used to estimate f_I. Specifically, a integer CFO metric is calculated as

$$M(i) = \sum_{l=-N_g}^{N_g-1}\left(\left|r_1[l+\hat{d}]\right| - \left|r_2[l+\hat{d}+N_t-i]\right|\right), \tag{44}$$

for $-2sf_{\max} \le i \le 2sf_{\max}$, and f_I is estimated as,

$$\hat{f}_I = \frac{\arg\min_i |M(i)|}{2s}. \tag{45}$$

C. Refined Timing Offset Estimation

As discussed in the previous section, a non-zero f_I causes a shift in the CIR region, creating a bias of sf_I samples in the coarse TO estimate. Once the estimate of the integer CFO ($\hat{f}_I$) is available, the bias can be removed. The unbiased TO estimate ($\tilde{d}$) is computed as

$$\tilde{d} = \hat{d} - \hat{f}_I s. \tag{46}$$

$$\hat{f}_{\text{frac}} = \frac{1}{2\pi}\,\text{Im}\left(\ln\left(\sum_{n=N_t-N_g}^{N_t-1} y[\hat{d}+n]y^*[\hat{d}+n+N] + \sum_{n=2N_t-N_g}^{2N_t-1} y[\hat{d}+m]y^*[\hat{d}+m+N]\right)\right) \tag{40}$$

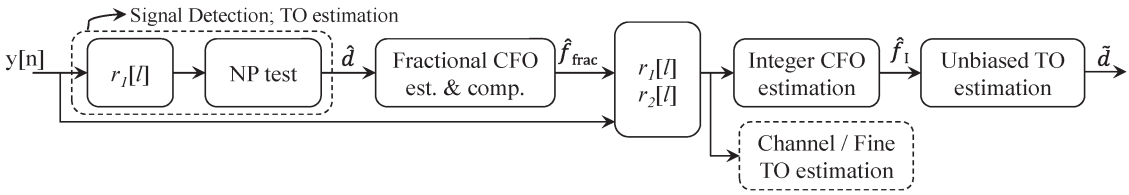

Fig. 3. Block diagram of the proposed downlink synchronization scheme.

Apart from integer CFO estimation, (42) and (43) also provide the CIR estimate, which can be used for fine TO estimation, as in [17].

This completes the discussion on synchronization using the proposed training block, and the block diagram of the proposed scheme is shown in Fig. 3. The detection and coarse timing synchronization procedures are entirely based on cross-correlation and threshold-based validation. In addition, after fractional CFO estimation and compensation, cross-correlation provides the integer CFO, the channel, and fine TO estimates. In the literature, integer CFO estimation is usually performed using correlation of the received training symbol in sub-carrier domain, as in [11], which increases the complexity and the latency of integer CFO estimation. Hence, as the hardware resources used for computing cross-correlations can be used for CFO, coarse TO, fine TO, and channel estimation, the proposed scheme is conducive to practical implementation.

VII. Simulation Results

In this section, we evaluate the performance of the proposed algorithms through Monte Carlo simulations and make comparisons with some of the existing approaches in the literature. Transmission is simulated in the form of packets, where each packet contains the preamble (training block) followed by 20 OFDM symbols carrying data. For training block detection tests, we simulate for $N = 64$, 128, and 256 with $u = -1$, which gives $s = 1$. For timing and CFO estimation, $N = 256$ is employed with $u = -1$, 85, and 51. The length of CP is $N_{\text{CP}} = \frac{N}{8}$ and $f_{\max} = 2$. The CFO for each iteration of the simulation is drawn randomly from $[-f_{\max}, f_{\max}]$. The channel is modeled as a Rayleigh fading channel with six taps and an exponential PDP given as $\sigma_p^2 = \frac{1}{\sum_{p=0}^{P-1} e^{-4\frac{p}{P}}} e^{-4\frac{p}{P}}$, $0 \le p \le P-1$ with unit average channel energy. The modulation scheme for OFDM symbols carrying data is Quadrature Phase-Shift Keying (QPSK). The number of samples used for noise variance estimation in (37) is $M = N$.

A. Performance of Training Block Detection

1) Performance of the Signal Detection Test in (30): Fig. 4 shows a comparison of the theoretical and the simulated results for the signal detection test in (30) with $N = 256$ and $u = -1$. Recall that the value of threshold γ' in (30) depends on CFO, SNR and channel PDP. Therefore, we calculate γ' through (32) for different values of target P_{FA}, SNR, and the aforementioned PDP with two cases for CFO. In the first case, we calculate γ' for $f = 0$ and simulate without CFO as the ideal benchmark. In the second case, we calculate γ' for a CFO of 0.5 while in simulation, CFO is chosen randomly from $[-f_{\max}, f_{\max}]$ for each iteration. As γ' is independent of integer CFOs, 0.5 is chosen as the worst case value for non-zero f_{F}. The probability of miss is calculated through simulations for each case and compared against the analytical values. As expected, a lower value of target P_{FA} results in a higher P_{MISS}. As shown in Fig. 4, the simulated points match well with the theoretical curves for zero CFO case. Moreover, the performance of non-zero CFO is very close to the zero CFO case. The slight degradation in the non-zero CFO case is because of the independence assumption made during the design of NP test in Section V.

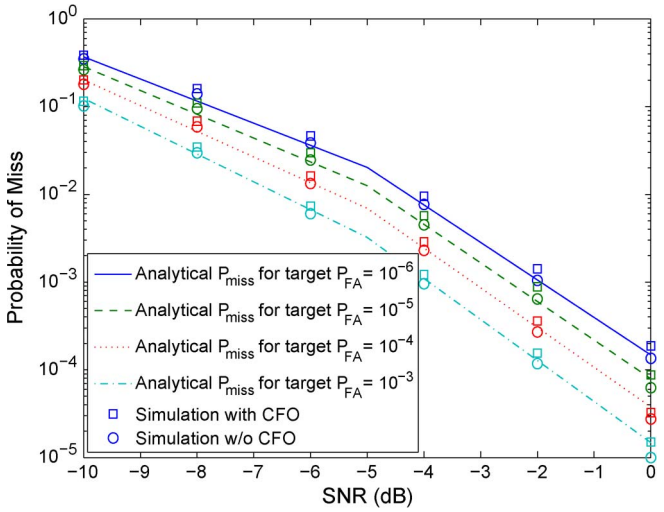

Fig. 4. Comparison of simulated and analytical P_{MISS} for different target P_{FA} values for the training block detection in (30); $N = 256$, $N_{\text{g}} = 32$, and $u = -1$.

2) Performance of the Simplified NP Test in (36): We now compare the performance of the original test in (30) and the simplified NP test in (36). Recall that the calculation of γ' in (35) for simplified NP test is independent of the CFO, channel PDP and noise variance. Hence, the value of γ' for simplified NP test changes only with the target P_{FA}. However, both tests require knowledge of the noise variance. Fig. 5 shows the P_{FA} obtained from simulations using γ' designed for different combinations of target P_{FA} values and the length N of the ZC sequence. For the simplified NP test, we present the performance both with perfect knowledge of noise variance and with its estimated value using (37). As shown, both original and simplified NP tests perform very close to the target P_{FA} for each value of SNR. Also the performance difference between the two tests is minimal when both test use ideal values of noise variance. However, the performance of simplified NP test with estimated noise variance is better than the target P_{FA} as compared to the perfect knowledge case. The gap between the performance of simplified NP test with and without perfect knowledge of noise variance decreases as the value of N

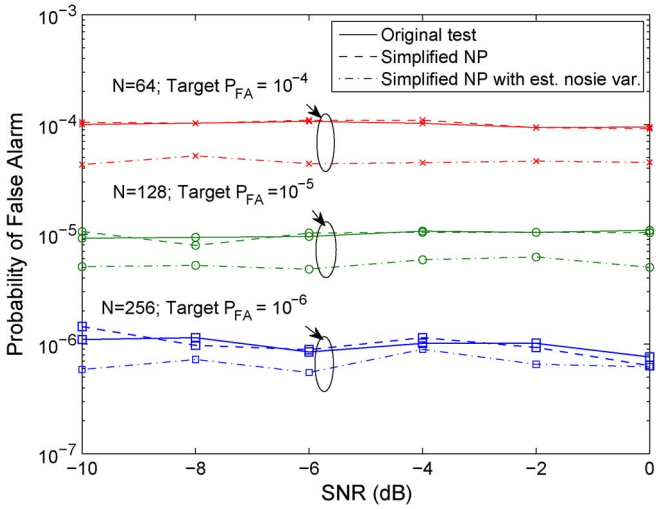

Fig. 5. Comparison of simulated P_{FA} of the original NP test, simplified NP test, and simplified NP test with noise variance estimation for different values of N and target P_{FA}.

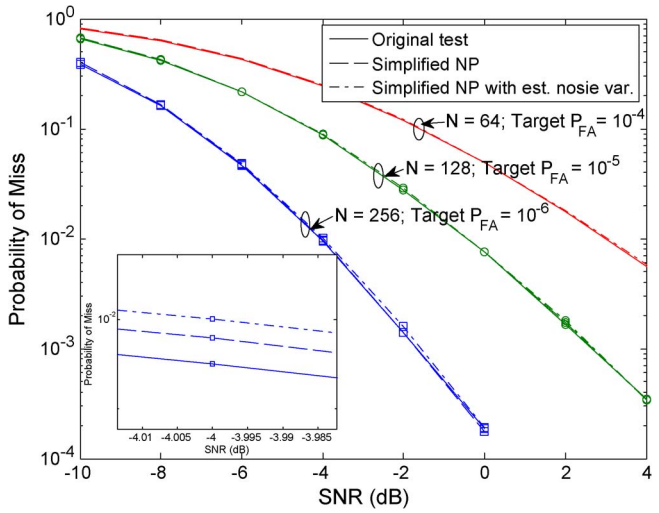

Fig. 6. Comparison of simulated P_{MISS} of the original NP test, simplified NP test, and simplified NP test with noise variance estimation for different values of N and target P_{FA}.

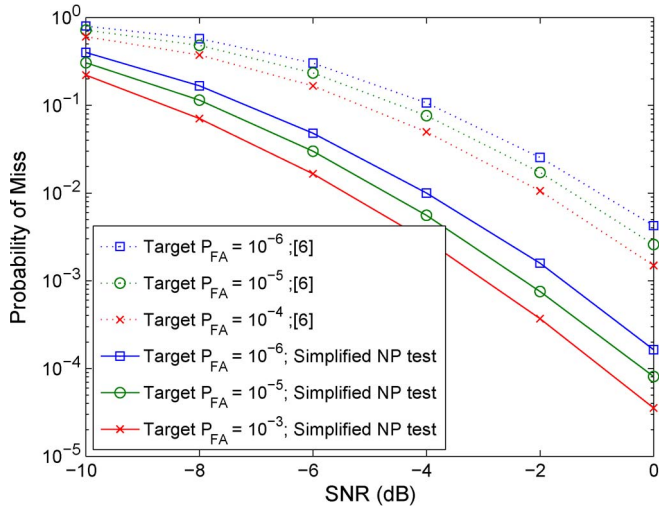

Fig. 7. Comparison of simulated P_{MISS} of the simplified NP test, and [6] for different target P_{FA} values; $N = 256$, $N_{\text{g}} = 32$, and $u = -1$.

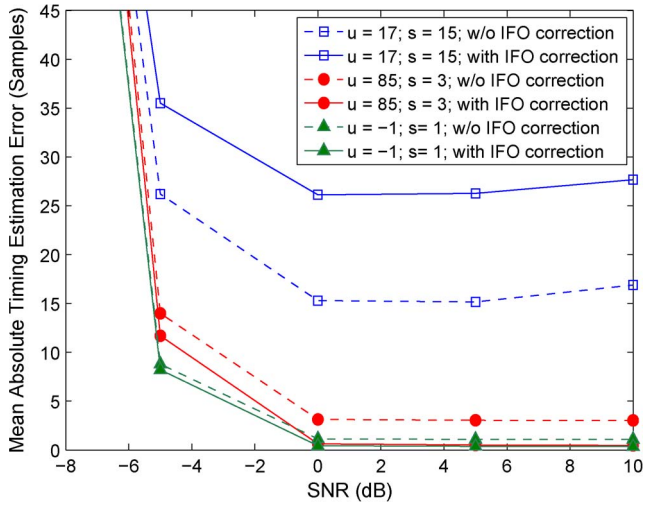

Fig. 8. Performance of coarse TO estimation using the proposed algorithm for different values of root index u.

increases because of increased noise variance estimation accuracy as $M = N$.

Fig. 6 shows the performance comparison in terms of P_{MISS} for different combinations of target P_{FA} values and the length N of the ZC sequence. It also shows the zoomed-in performance at SNR of -4 dB for $N = 256$ case. Again, the original test assumes perfect knowledge of noise variance while the simplified NP test is simulated for both perfect knowledge case and the estimated noise variance case. As shown, the performance of simplified NP test, with and without perfect knowledge of noise variance, is very close to the original test for all values of target P_{FA} and N. The performance of simplified NP test is slightly degraded as compared to the original test. However, the degradation is minimal, which shows that the approximation employed in deriving the simplified NP test in Section V-A1, i.e., $\sigma^2_{\tilde{w}} \ll \sigma^2_{\tilde{k}}$ has negligible effect on its performance. Also the performance of simplified NP test with estimated noise variance is further degraded as compared to the perfect knowledge case, as shown in the magnified sub-figure. However, this performance degradation in P_{MISS} also provides an improvement in P_{FA} as discussed earlier for Fig. 5.

Fig. 7 presents the performance comparison, in terms of P_{MISS}, of simplified NP test with estimated noise variance against the signal detection algorithm in [6] for $N = 256$ and different values of target P_{FA}. As shown, the performance of simplified NP test exhibits a considerable improvement in performance as compared to [6]. These results show that the proposed signal detection schemes are indeed robust to large values of CFOs and the detection performance is superior to the schemes proposed in the literature. Moreover, the simplified NP test results in negligible performance degradation as compared to the original test. Hence, we will use only simplified NP test and its corresponding γ' values for the following simulation results.

B. Performance of Timing Synchronization

In Fig. 8, we present the performance of proposed coarse timing synchronization in terms of mean absolute TO estimation error using the proposed simplified NP test. The value of γ'

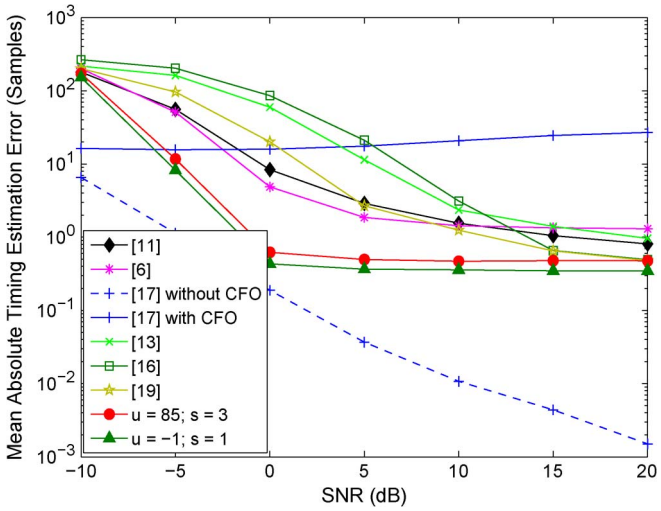

Fig. 9. Performance of the proposed TO estimation compared with existing schemes.

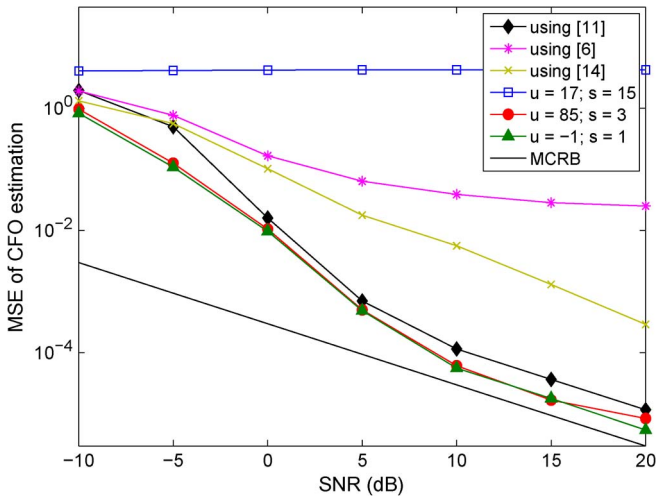

Fig. 10. Performance of CFO estimation using the proposed algorithm for different values of root index u.

for the proposed test is designed for a target P_{FA} of 10^{-6} and the performance is evaluated, with and without the integer offset correction in (46), for three different root indices that are $u = -1$, 85, and 17, which result in $s = 1$, 3, and 15 samples, respectively. As $sf_{\max} = 30$ for $u = 17$, the TO estimates do not always lie in the ISI-free region. Thus, $u = 17$ is not a reasonable choice for the aforementioned system parameters and poor performance is expected in this case. On the other hand, both $u = -1$ and 85 are good choices. As shown in Fig. 8, without integer-offset-based correction, both $s = 1$ and 3 show a bias in TO estimation. However, integer-offset-based correction removes the bias in both cases while $u = -1$ with a smaller value of s offers better performance for lower SNRs. The performance for $u = 17$, both with and without IFO-based correction, is poor as expected.

In Fig. 9, we compare the performance of the proposed algorithms with the timing synchronization methods in [6], [11], [13], [16], [17], [19]. As the timing metric for [11] shows a plateau, which causes ambiguity in TO estimation, we apply a moving average window equal to the size of the plateau to improve the TO estimate. As shown, the proposed algorithm for feasible root indices offers a significant improvement in performance specially for lower SNRs, which shows the effectiveness of the proposed algorithm. When simulating fine timing estimation in [17], we assume that the receiver already knows the coarse timing estimate and the cross-correlation region for all SNR values. Thus, the performance of [17] without CFO outperforms the proposed methods. However, in the presence of CFO, the performance degrades severely, which shows that the algorithm is not robust to CFOs. The schemes in [13], [16], [19] provide a sharp peak in timing metrics for flat fading channels but for multi-path channels, the performance degrades.

C. Performance of CFO Estimation

In Fig. 10, we present the performance of coarse CFO estimation, in terms of mean square error (MSE) of CFO estimation $\left(E\left[|f-\hat{f}|^2\right]\right)$, using the proposed algorithm and its comparison with the coarse CFO estimation in [6], [11], [14]. The values of root indices used in the simulation are the same as the ones in Section VII-B. We also plot the modified Cramer-Rao bound (MCRB) [35] as an absolute reference for CFO estimation. As shown, in addition to better coarse TO estimation, root indices -1 and 85 also result in better CFO estimation performance. Moreover, the MSEs for $u = -1$ and 85 are better than the CFO estimation proposed in [6], [11], [14], particularly for lower SNRs and the performance is closer to MCRB as the SNR increases. The CFO estimation in [6], showing an error floor for high SNR values, requires fine CFO estimation for further performance improvement. The performance for infeasible root index $u = 17$ again suffers ahigh error floor similar to its TO estimation performance. This is because the performance of CFO estimation in Section VI depends on successful TO estimation. Integer CFO estimation in (45) requires a TO estimate within the ISI-free region while the performance of fractional CFO estimation in (40) degrades with deviation of TO estimate from the ideal starting point. As $u = 17$ results in $s = 15$, the TO estimate does not always lie in the ISI-free region and therefore, CFO estimation performance for $u = 17$ exhibits an error floor.

D. Comparison of Bit Error-Rate

Fig. 11 shows the comparison of the proposed synchronization scheme with the methods proposed in [6], [11] in terms of bit error-rate (BER). We simulate four different feasible root indices $u = -1$, 85, 51, and 73 with $s = 1$, 3, 5, and 7, respectively. The maximum deviation from the ideal TO estimate is 14 samples for $u = 73$ with $s = 7$ and $f_{\max} = 2$, which is still within the ISI-free region. We also show the BER performance of the system with ideal synchronization, which implies that the receiver has the exact knowledge of the TO and the CFO. As shown, the performance of the proposed training block is similar for all feasible root indices and it is also significantly better than the performance of [6], [11].

The simulation results show the effectiveness of the proposed algorithms for detection, timing, and frequency synchronization. It shows that if the root indices of the ZC sequences are carefully chosen according to (11), cross-correlation-based

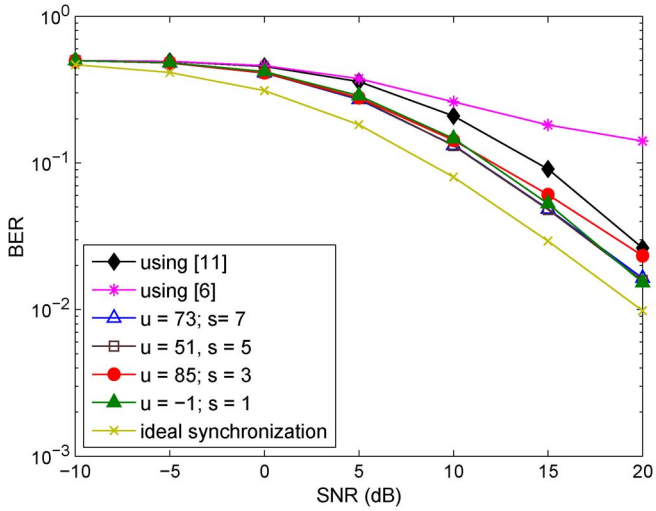

Fig. 11. Bit error rate performance of the proposed algorithm for different values of root index u.

timing synchronization achieves robustness to integer CFOs and offers considerable improvements specially in lower SNR regimes.

VIII. Conclusion

We presented a coarse timing offset and integer CFO estimation method for downlink OFDM systems. The training block, consisting of two suitably chosen Zadoff-Chu sequences, reduced the sensitivity to integer CFOs and allowed coarse TO estimate to reside within the ISI-free region. We presented the criterion for selecting the root index of the Zadoff-Chu sequence to accommodate a certain maximum CFO. We also presented a training block detection test and its approximation to alleviate the dependency on the multi-path channel profile and the CFO. The proposed detection and coarse timing synchronization schemes, along with the CFO estimation and the subsequent refinement of the TO estimate, offer better performance than the existing schemes in the literature.

Appendix

A. Proof of Proposition 1

$l_2 = l_1 + (l_1 - N_g - d)$ satisfies the claim as

$$\begin{aligned} u(l_2 - N_g - d) + 2 &= u\left(l_1 + (l_1 - N_g - d) - N_g - d\right) + 2 \\ &= 2u(l_1 - N_g - d) + 2 = 2m_1 N \\ &= m_2 N. \end{aligned}$$

Similarly,

$$\begin{aligned} u(l_{i+1} - N_g - d) + i + 1 &= u\left(l_i + (l_1 - N_g - d) - N_g - d\right) \\ &\quad + i + 1 \\ &= u(l_i - N_g - d) + i + m_1 N \\ &= u(l_{i-1} - N_g - d) + i - 1 \\ &\quad + 2m_1 N \\ &\quad \vdots \\ &= u(l_1 - N_g - d) + 1 + im_1 N \\ &= (i+1)m_1 N. \end{aligned}$$

■

B. Proof of Proposition 2

Assume that there exists an index l_{i1} such that,

$$u(l_{i1} - N_g - d) + i = m_{i1} N$$

for some integer m_{i1} while l_{i1} lies in $\mathcal{R}_{\text{cc}}$, i.e., $d \le l_{i1} \le d + 2N_g$, and $N_g < \frac{N}{2}$, which is usually the case. Now assume that there exists another l_{i2} such that

$$u(l_{i2} - N_g - d) + i = m_{i2} N$$

for the same i, but some integer $m_{i2} \neq m_{i1}$. Then,

$$u(l_{i2} - l_{i1}) = (m_{i2} - m_{i1})N$$

or

$$\frac{u}{N} = \frac{m_{i2} - m_{i1}}{l_{i2} - l_{i1}}.$$

As u is relatively prime to N, the minimum possible value of $(l_{i2} - l_{i1})$ is $\pm N$ or $l_{i2} = l_{i1} \pm N$. Therefore, both l_{i2} and l_{i2} cannot lie in $\mathcal{R}_{\text{cc}}$ at the same time while outside $\mathcal{R}_{\text{cc}}$, the linear correlation is no longer equal to the circularcorrelation. Hence, the indices in $\mathcal{R}_{\text{CIR}}$ are unique. ■

References

[1] *IEEE Standard for Information Technology-Telecommunications and Information Exchange Between Systems Local and Metropolitan Area Networks-Specific Requirements Part 11: Wireless LAN Medium Access Control (MAC) and Physical Layer (PHY) Specifications*, IEEE Std. 802.11-2012 (Revision of IEEE Std. 802.11-2007), Mar. 2012, pp. 1-2793.

[2] *IEEE Standard for Air Interface for Broadband Wireless Access Systems*, IEEE Std. 802.16-2012 (Revision of IEEE Std. 802.16-2009), Aug. 2012, pp. 1-2542.

[3] "Technical specification group radio access network; Physical layer aspects for evolved universal terrestrial radio access (UTRA) (Release 7)," Cedex, France, 3GPP TR 25.814, V7.1.0, Sep. 2006.

[4] U. Reimers, "DVB-T: The COFDM-based system for terrestrial television," *Electron. Commun. Eng. J.*, vol. 9, no. 1, pp. 28–32, Feb. 1997.

[5] M. Speth, S. Fechtel, G. Fock, and H. Meyr, "Optimum receiver design for wireless broad-band systems using OFDM. I," *IEEE Trans. Commun.*, vol. 47, no. 11, pp. 1668–1677, Nov. 1999.

[6] H. Minn, V. Bhargava, and K. Letaief, "A robust timing and frequency synchronization for OFDM systems," *IEEE Trans. Wireless Commun.*, vol. 2, no. 4, pp. 822–839, Jul. 2003.

[7] B. Yang, K. Letaief, R. Cheng, and Z. Cao, "Timing recovery for OFDM transmission," *IEEE J. Sel. Areas Commun.*, vol. 18, no. 11, pp. 2278–2291, Nov. 2000.

[8] A. Coulson, "Maximum likelihood synchronization for OFDM using a pilot symbol: Algorithms," *IEEE J. Sel. Areas Commun.*, vol. 19, no. 12, pp. 2486–2494, Dec. 2001.

[9] M. Morelli, C. Kuo, and M. Pun, "Synchronization techniques for orthogonal frequency division multiple access (OFDMA): A tutorial review," *Proc. IEEE*, vol. 95, no. 7, pp. 1394–1427, Jul. 2007.

[10] P. H. Moose, "A technique for orthogonal frequency division multiplexing frequency offset correction," *IEEE Trans. Commun.*, vol. 42, no. 10, pp. 2908–2914, Oct. 1994.

[11] T. Schmidl and D. Cox, "Robust frequency and timing synchronization for OFDM," *IEEE Trans. Commun.*, vol. 45, no. 12, pp. 1613–1621, Dec. 1997.

[12] F. Tufvesson, O. Edfors, and M. Faulkner, "Time and frequency synchronization for OFDM using PN-sequence preambles," in *Proc. IEEE 50th Veh. Technol. Conf.*, Amsterdam, Netherlands, Sep. 1999, vol. 4, pp. 2203–2207.

[13] B. Park, H. Cheon, C. Kang, and D. Hong, "A novel timing estimation method for OFDM systems," *IEEE Commun. Lett.*, vol. 7, no. 5, pp. 239–241, May 2003.

[14] M. Morelli and U. Mengali, "An improved frequency offset estimator for OFDM applications," in *Proc. Commun. Theory Mini-Conf.*, Vancouver, BC, Canada, Jun. 1999, pp. 106–109.
[15] K. Shi and E. Serpedin, "Coarse frame and carrier synchronization of OFDM systems: A new metric and comparison," *IEEE Trans. Wireless Commun.*, vol. 3, no. 4, pp. 1271–1284, Jul. 2004.
[16] G. Ren, Y. Chang, H. Zhang, and H. Zhang, "Synchronization method based on a new constant envelop preamble for OFDM systems," *IEEE Trans. Broadcast.*, vol. 51, no. 1, pp. 139–143, Mar. 2005.
[17] C.-L. Wang and H.-C. Wang, "On joint fine time adjustment and channel estimation for OFDM systems," *IEEE Trans. Wireless Commun.*, vol. 8, no. 10, pp. 4940–4944, Oct. 2009.
[18] C.-L. Wang and H.-C. Wang, "Optimized joint fine timing synchronization and channel estimation for MIMO systems," *IEEE Trans. Commun.*, vol. 59, no. 4, pp. 1089–1098, Apr. 2011.
[19] H. Abdzadeh-Ziabari and M. Shayesteh, "A novel preamble-based frame timing estimator for OFDM systems," *IEEE Commun. Lett.*, vol. 16, no. 7, pp. 1121–1124, May 2012.
[20] M. Gul, S. Lee, and X. Ma, "Robust synchronization for OFDM employing Zadoff-Chu sequence," in *Proc. 46th Annu. CISS*, Princeton, NJ, USA, Mar. 2012, pp. 1–6.
[21] J.-J. van de Beek, M. Sandell, and P. Börjesson, "ML estimation of time and frequency offset in OFDM systems," *IEEE Trans. Signal Process.*, vol. 45, no. 7, pp. 1800–1805, Jul. 1997.
[22] X. Ma, C. Tepedelenlioğlu, G. Giannakis, and S. Barbarossa, "Non-data-aided carrier offset estimators for OFDM with null subcarriers: Identifiability, algorithms, performance," *IEEE J. Sel. Areas Commun.*, vol. 19, no. 12, pp. 2504–2515, Dec. 2001.
[23] X. Ma, G. Giannakis, and S. Barbarossa, "Non-data-aided frequency-offset and channel estimation in OFDM and related block transmissions," in *Proc. IEEE Int. Conf. Commun.*, Helsinki, Finland, 2001, vol. 6, pp. 1866–1870.
[24] U. Tureli, H. Liu, and M. Zoltowski, "OFDM blind carrier offset estimation: ESPRIT," *IEEE Trans. Commun.*, vol. 48, no. 9, pp. 1459–1461, Sep. 2000.
[25] H. Bölcskei, "Blind estimation of symbol timing and carrier frequency offset in wireless OFDM systems," *IEEE Trans. Commun.*, vol. 49, no. 6, pp. 988–999, Jun. 2001.
[26] M. Luise, M. Marselli, and R. Reggiannini, "Low-complexity blind carrier frequency recovery for OFDM signals over frequency-selective radio channels," *IEEE Trans. Commun.*, vol. 50, no. 7, pp. 1182–1188, Nov. 2002.
[27] B. Park, H. Cheon, E. Ko, C. Kang, and D. Hong, "A blind OFDM synchronization algorithm based on cyclic correlation," *IEEE Signal Process. Lett.*, vol. 11, no. 2, pp. 83–85, Jan. 2004.
[28] Y. Yao and G. Giannakis, "Blind carrier frequency offset estimation in SISO, MIMO, multiuser OFDM systems," *IEEE Trans. Commun.*, vol. 53, no. 1, pp. 173–183, Feb. 2005.
[29] D. Chu, "Polyphase codes with good periodic correlation properties," *IEEE Trans. Inf. Theory*, vol. 18, no. 4, pp. 531–532, Jul. 1972.
[30] ITU Recommendations M.1225 Guidelines for evaluation of radio transmission technologies for IMT-2000 1997, ITU Recommendations M.1225.
[31] K. Manolakis, D. Gutierrez Estevez, V. Jungnickel, W. Xu, and C. Drewes, "A closed concept for synchronization and cell search in 3GPP LTE systems," in *Proc. IEEE Wireless Commun. Netw. Conf.*, Budapest, Hungary, Apr. 2009, pp. 1–6.
[32] S. Kay, *Fundamentals of Statistical Signal Processing*, vol. II, *Detection Theory*. Upper Saddle River, NJ, USA: Prentice-Hall, 1998.
[33] S. Ross, *Introduction to Probability Models*, 10th ed. New York, NY, USA: Academic, 2009.
[34] R. Valcarce and C. Mosquera, "Maximum likelihood SNR estimation for asynchronously oversampled OFDM signals," in *Proc. IEEE 9th Workshop Signal Process. Adv. Wireless Commun.*, Recife, Brazil, Jul. 2008, pp. 26–30.
[35] A. D'Andrea, U. Mengali, and R. Reggiannini, "The modified Cramer-Rao bound and its application to synchronization problems," *IEEE Trans. Commun.*, vol. 42, no. 234, pp. 1391–1399, Feb. 1994.

Malik Muhammad Usman Gul received the B.E and M.S. degrees in electrical engineering from the National University of Sciences and Technology, Pakistan, in 2007 and 2009, respectively. He received the Ph.D. degree from Georgia Institute of Technology, Atlanta, GA, USA, in 2014. Since 2014, he has been a Staff RF & Communications Engineer at National Instruments Corporation. His research interests include design, analysis, and prototyping of synchronization and detection algorithms for next-generation wireless networks.

Xiaoli Ma (SM'09) received the B.S. degree in automatic control from Tsinghua University, Beijing, China, in 1998, the M.S. degree in electrical engineering from the University of Virginia, Charlottesville, VA, USA, in 2000, and the Ph.D. degree in electrical engineering from the University of Minnesota, Minneapolis, MN, USA, in 2003. After receiving the Ph.D. degree, she joined the Department of Electrical and Computer Engineering, Auburn University, where she served as an Assistant Professor until Dec. 2005. Since Jan. 2006, she has been with the School of Electrical and Computer Engineering, Georgia Tech, where she is currently a Professor. In July 2012, she was appointed a Co-director of the Georgia Tech Ultra Wideband Center of Excellence. She was awarded the Lockheed Martin Aeronautics Company Dean's Award for Teaching Excellence by the College of Engineering in 2009, and the Outstanding Junior Faculty Award by the School of Electrical and Computer Engineering in 2010, at Georgia Tech. Her research focuses on networking and communications, including network performance analysis, transceiver designs for wireless time- and frequency-selective channels, channel estimation and equalization algorithms, carrier frequency synchronization for OFDM systems, performance analysis and cooperative designs for wireless networks. She serves as a Senior Area Editor for IEEE SIGNAL PROCESSING LETTERS since 2014 and *Elsevier Digital Signal Processing* since June 2012, and has been an Associate Editor for IEEE SIGNAL PROCESSING LETTERS (2007–2009) and IEEE TRANSACTIONS ON WIRELESS COMMUNICATIONS (2008–2013).

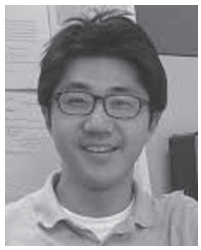

Sungeun Lee received the B.S. degree in electrical and electronic engineering and in computer science and industrial system engineering from the Yonsei University, Seoul, Korea, in 2002, and the M.S. and Ph.D. degrees from the Yonsei University, Seoul, in 2004 and 2009, respectively, all in electrical and electronic engineering. From 2009 to 2012, he was a Postdoctoral Research Fellow at Georgia Institute of Technology, GA, USA. He also served as a Principal Investigator of the National Science Foundation at Ratrix Technologies, LLC in 2012. Since 2013, he has been serving as a Senior Staff Engineer at Broadcom Corporations. His research interest includes the digital signal processing on the wireless communication systems such as synchronization, channel estimation, MIMO detection, and the architecture design for the implementation of the wireless system.